International Journal of Heat and Technology
Vol. 44, No. 2, April, 2026, pp. 873-887
Journal homepage: http://iieta.org/journals/ijht

Natural Convection in Hexagonal Coaxial Cavities with Localized Heat Sources: 3D Analysis and Material Effects (Al vs. Cu)

Amor Begar, Abdelhakim Begar*, Mohamed Said Chebbah

Department of Mechanical Engineering, University of Biskra, Biskra 07000, Algeria

Corresponding Author Email: a.begar@univ-biskra.dz

https://doi.org/10.18280/ijht.440237

Received: 26 January 2026
Revised: 9 April 2026
Accepted: 17 April 2026
Available online: 30 April 2026

Keywords:
natural convection, hexagonal coaxial cavity, localized heat sources, Rayleigh number, Nusselt number, three-dimensional numerical simulation, heat transfer enhancement, ANSYS Fluent

ABSTRACT

This study presents a comprehensive numerical investigation of natural convection in hexagonal coaxial cavities with localized internal heat sources, a configuration relevant to compact thermal management systems. The objective is to analyze the coupled effects of heat source configuration (single vs. dual) and material properties (aluminum vs. copper) on heat transfer performance, which remains insufficiently explored. Two-dimensional (2D) and three-dimensional (3D) simulations are performed using ANSYS Fluent under the Boussinesq approximation for Rayleigh numbers ranging from 10^3 to 10^6. The results show a transition from conduction-dominated to convection-dominated regimes with increasing Rayleigh number. In dual-source configurations, plume interactions enhance convective structures, leading to improved thermal mixing. Quantitatively, copper heat sources enhance heat transfer performance, increasing the average Nusselt number by up to 20% and maximum velocity magnitude by approximately 25% compared to aluminum at high Rayleigh numbers. Additionally, copper reduces core temperature by nearly 12%, demonstrating superior thermal diffusion capability. New empirical power-law correlations relating the average Nusselt number to the Rayleigh number are proposed for different configurations, providing predictive tools for engineering applications such as compact heat exchangers and passive cooling systems.

1. INTRODUCTION

Natural convection in complex enclosures plays a pivotal role in thermal management systems, including heat exchangers, microelectronic devices, and solar thermal collectors. Among various geometric configurations, coaxial enclosures have garnered increasing interest for their potential in compact and modular designs. While circular and rectangular coaxial cavities have been extensively studied, hexagonal configurations remain largely unexplored, despite their relevance for modular thermal designs [1-3].

Recent studies have investigated natural convection in polygonal and hexagonal enclosures, including the effects of inner cylinders, fins, and discrete heat sources on flow structure and heat transfer enhancement [4-8]. However, configurations involving localized internal heat sources in hexagonal coaxial cavities remain insufficiently explored. In particular, the interaction between thermal plumes generated by single and dual internal heat sources within such geometries has not been systematically analyzed.

In addition, the thermal conductivity of the source material is a decisive factor, governing local temperature gradients and overall heat transfer performance. Furthermore, while several studies have compared aluminum and copper in classical heat sink designs [9], this work represents the first quantitative evaluation of their impact in dual-source hexagonal coaxial geometries. Copper, with nearly twice the conductivity of aluminum, promotes more efficient heat dissipation. However, aluminum remains dominant in industrial applications because its lower density and cost offer a practical balance between performance and affordability. This trade-off highlights the importance of numerical studies that quantify the relative gains of copper versus aluminum in confined convection systems [10, 11]. Similar trends were reported in photovoltaic thermal management, where aluminum and copper heat sinks showed distinct trade-offs in efficiency and cost [9]. However, comparative studies that assess their thermal performance in dual-source configurations are limited.

Recent findings further highlight the role of surface coatings in enhancing the passive cooling performance of aluminum and copper heat sinks, confirming that both material conductivity and surface treatment govern overall thermal efficiency [12].

The majority of previous numerical investigations have been conducted in two dimensions. Yet, three-dimensional (3D) effects such as vortex formation, secondary flow, and spatial heat plume development are essential for accurately capturing the behavior of natural convection in complex geometries [13]. Hence, a multidimensional analysis is necessary for reliable thermal design in realistic applications.

Hexagonal cavities, often encountered in natural systems such as honeycombs and mineral structures, are investigated here for their potential in passive thermal design.

The objective of the present study is to conduct a detailed

numerical investigation of natural convection in a hexagonal coaxial cavity, considering both single and dual internal isothermal sources, and comparing the thermal behavior of copper and aluminum as source materials. An additional contribution of this study is the derivation of new empirical Nusselt–Rayleigh correlations, which extend existing models for polygonal cavities [14] and provide predictive tools for engineering applications. The analysis spans both Two-dimensional (2D) and 3D simulations over a wide range of Rayleigh numbers (10^3 to 10^6), capturing the transition from conduction to convection-dominated regimes. The results are interpreted in terms of temperature fields, flow structures, and Nusselt number distributions. Furthermore, empirical correlations are proposed to predict the global heat transfer performance, enabling better integration of such geometries into future thermal systems.

This work fills several gaps in the literature by offering a comprehensive assessment of the geometric, physical, and material parameters affecting natural convection in coaxial enclosures, and it contributes to the design and optimization of compact, high-efficiency heat transfer devices.

In addition to its relevance for compact thermal systems and electronic cooling, the configuration studied in this work presents promising applications in mining engineering, metallurgical processes, and mechanical engineering.

In underground mining environments, passive thermal regulation helps improve safety and energy efficiency. In metallurgy, controlling localized heat transfer enhances material quality and process stability. Meanwhile, in mechanical systems, the studied coaxial geometries and thermal correlations can be applied to the design of compact heat exchangers, cooling units, and thermally optimized components.

The numerical results obtained here can thus support the development of effective thermal management solutions across these engineering domains.

Unlike previous works limited to 2D analyses of polygonal cavities [15], the present study provides a systematic 2D–3D comparison combined with material effects (Al vs. Cu), filling a clear gap in the literature.

2. PHYSICAL MODEL AND GEOMETRY

The studied configuration consists of a hexagonal coaxial cavity formed by an outer hexagonal wall and an inner cylindrical or prismatic cavity. The system is designed to investigate natural convection induced by localized internal heating, with applications in compact thermal devices and energy systems.

2.1 Geometry description

As shown in Figure 1, the computational domain represents a vertical coaxial cavity with the following geometric specifications:

• Outer hexagonal enclosure with a side length chosen to preserve a constant hydraulic diameter across configurations.

• Inner cavity includes either a single central isothermal source or two symmetrically placed heat sources.

• The total height of the domain is Lout = 2.12 m, while the height of each heat source is Lin = 1.06 m.

The width and vertical position of the source(s) are chosen to maintain geometric symmetry and induce well-structured convective cells. Two configurations are studied:

• Single heat source (SHS): One centrally placed source, representing classical thermal loading.

• Dual heat sources (DHS): Two equal isothermal zones symmetrically placed along the vertical axis.

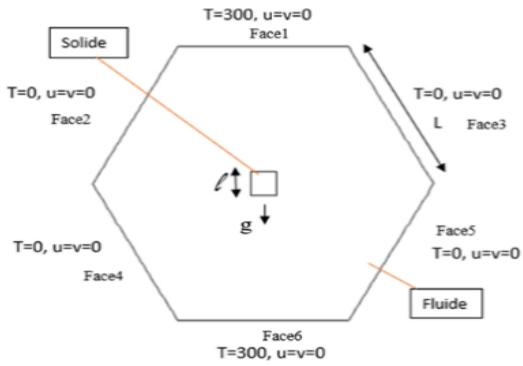

Figure 1. Schematic representation of the concentric hexagonal annulus used in the numerical simulation, showing the thermal boundary conditions and geometric parameters

2.2 Materials and thermophysical properties

The working fluid is air, treated as an incompressible Newtonian fluid with constant thermophysical properties:

• Density: $\rho = 1.225$ kg/m^3

• Thermal conductivity: $k = 0.0262$ W/m

• Dynamic viscosity: $\mu = 1.7894 \times 10^{-5}$ kg/m

• Specific heat: $cp = 1007$ J/kg

• Thermal expansion coefficient: $\beta = 1/T0$, with $T0 = 300$ K

The heat sources are modeled using two different solid materials for comparison:

• Aluminum (Al): $k_{Al} = 205$ W/m

• Copper (Cu): $k_{Cu} = 385$ W/m

These materials were chosen due to their widespread use in thermal systems and their contrasting thermal conductivities, which allow evaluation of material-dependent thermal response.

2.3 Flow regime and dimensionless parameters

Natural convection in the cavity is driven by temperature differences between the heated inner source(s) and the cold outer wall. The problem is governed by the Rayleigh number:

$$Ra = \frac{g\beta(T_{hot} - T_{cold})L}{\vartheta\alpha}$$

Simulations were performed for a range of Ra from 103 to 106, covering both conduction-dominated and convection-dominated regimes.

3. NUMERICAL METHOD AND VALIDATION

3.1 Numerical method

The numerical simulation of natural convection within concentric hexagonal annuli was carried out using a finite volume method based on the discretization of the incompressible Navier–Stokes and energy equations under the Boussinesq approximation. A staggered grid arrangement was

adopted, where velocity components and scalar variables (pressure, temperature) are stored at different spatial locations to improve stability and accuracy.

Spatial discretization was carried out using a second-order central difference scheme for diffusion terms, while first-order upwind or second-order QUICK schemes were applied for convection, depending on the flow regime. The pressure–velocity coupling was resolved via the SIMPLE algorithm. Convergence was considered achieved when the residuals for all governing equations dropped below 10^{-6}, and the normalized temperature and velocity fields reached a steady-state profile.

Boundary conditions were imposed as follows:

• No-slip condition on all solid boundaries.

• Isothermal walls: the inner cylinder was maintained at a fixed hot temperature (Th), and the outer enclosure at a cold temperature (Tc).

• The Rayleigh number (Ra) was varied from 10^3 to 10^6, and the aspect ratio ($AR = \frac{L_{in}}{L_{out}}$) was fixed at 0.2 for the validation phase.

3.2 Validation of the numerical model

To ensure the accuracy and reliability of the present numerical model, a validation study was carried out by comparing the numerical results obtained in this work with the benchmark results reported by Alapati [15].

In the reference work, natural convection in a concentric hexagonal annulus was investigated numerically using a hybrid computational approach based on the Lattice Boltzmann Method (LBM), the Smoothed Profile Method (SPM), and a finite-difference method for solving the energy equation. In order to perform a consistent comparison, the same geometric configuration and boundary conditions were adopted in the present simulations.

The aspect ratio was fixed at AR = 0.2, and two representative Rayleigh numbers were considered:

$$Ra = 10^3 \text{ and } Ra = 10^6$$

These Rayleigh numbers correspond to two distinct heat transfer regimes: the conduction-dominated regime and the convection-dominated regime.

Figure 2 presents a comparison between the temperature contours obtained in the present numerical simulations and those reported in the reference study.

At Ra = 10^3, heat transfer inside the annular cavity is mainly governed by thermal conduction. The isotherms remain smooth and nearly concentric around the heated inner surface, indicating very weak fluid motion. The present numerical results reproduce this behavior accurately and show a strong agreement with the reference results.

At Ra = 10^6, buoyancy forces become dominant, and strong convective circulation develops inside the cavity. As a result, the isotherms become significantly distorted and a thermal plume forms above the heated region. The present numerical simulations successfully capture these characteristic features of the convection-dominated regime.

As shown in Figure 2, the overall structure of the temperature field predicted in the present study closely matches the reference results reported in the literature, demonstrating the capability of the present numerical approach to accurately reproduce the thermal behavior of natural convection in hexagonal annular geometries.

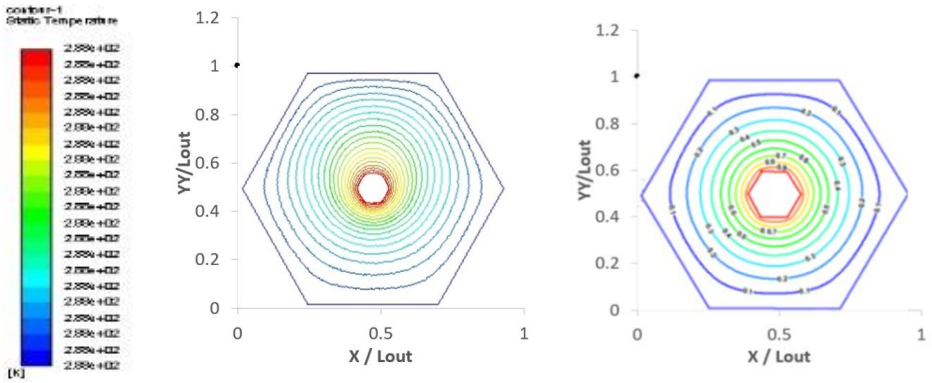

(a) Ra = 1000

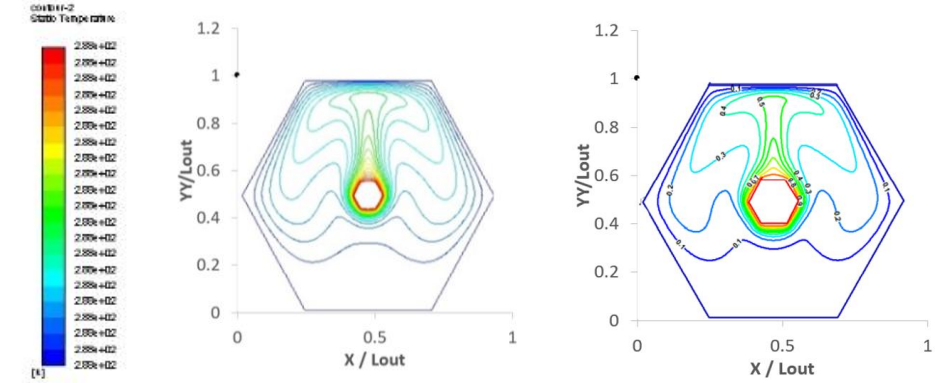

(b) Ra = 10^6

Figure 2. Comparison of isotherm contours in a concentric hexagonal annulus for Ra = 10^3 and Ra = 10^6 with AR = 0.2. Left: present numerical results; Right: reference results from Alapati [15]

In addition to the qualitative comparison, a quantitative validation was also performed using the average Nusselt number along the heated surface. The comparison between the present results and the benchmark data reported in the reference study is summarized in Table 1.

Table 1. Comparison of average Nusselt numbers with reference results

Rayleigh Number (Ra)	Nu_{ref} (Alapati)	$Nu_{present}$	Error (%)
10^4	2.042	2.08	1.86
10^5	3.714	3.79	2.04
10^6	5.959	6.10	2.36

The quantitative comparison presented in Table 1 shows that the deviation between the present numerical predictions and the benchmark data remains below 3%, which is considered acceptable for numerical simulations of natural convection problems.

These results confirm the reliability and accuracy of the numerical model used in this work, and therefore, the model can be confidently applied to investigate the heat transfer characteristics of the hexagonal coaxial cavity configurations considered in the present study.

4. RESULTS AND DISCUSSION

This section presents a comprehensive analysis of the numerical results obtained from both 2D and 3D simulations of natural convection in a hexagonal coaxial cavity. The investigation considers the effects of heat source configuration (single vs. dual), dimensionality (2D vs. 3D), and thermal conductivity of the source material (Aluminum vs. Copper) over a wide range of Rayleigh numbers (10^3–10^6). The discussion is organized to progressively address geometric, thermal, and material influences on the convective flow structure and heat transfer performance.

4.1 Effect of Rayleigh number in 2D – Single heat source

The 2D simulations with a single internal isothermal heat source reveal a typical transition from diffusion-dominated to convection-dominated regimes as the Rayleigh number (Ra) increases from 10^3 to 10^6. At Ra = 10^3, nearly parallel isotherms (Figure 3(a)-(d)) and stagnant velocity fields (Figure 3(e)-(h)) confirmed that heat transfer was dominated by pure conduction, since buoyancy forces were too weak to generate significant motion. This behavior is characteristic of low Rayleigh numbers, where thermal transport occurs almost exclusively by diffusion, and is consistent with the conduction-dominated regimes reported in benchmark studies such as Alapati [15].

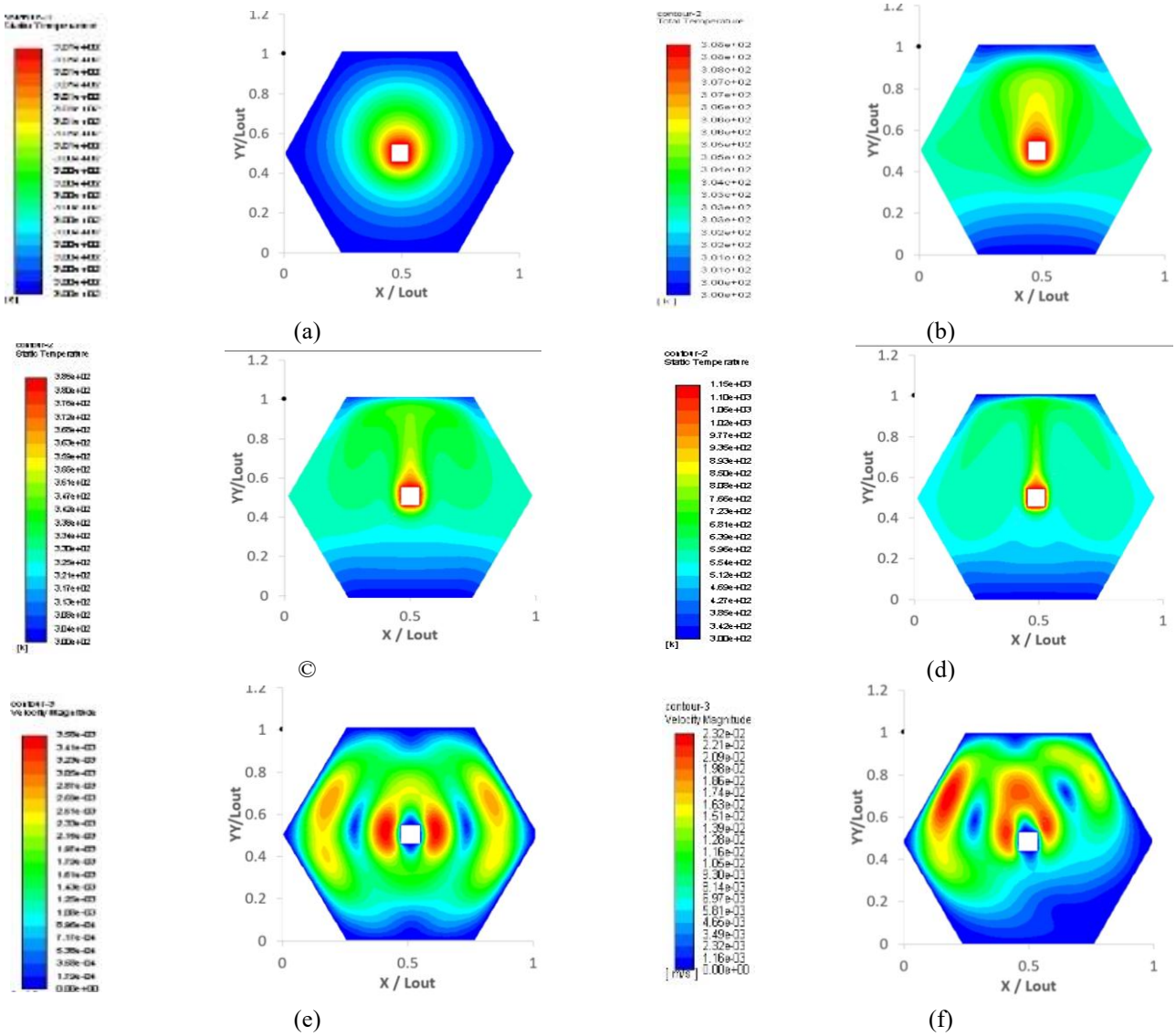

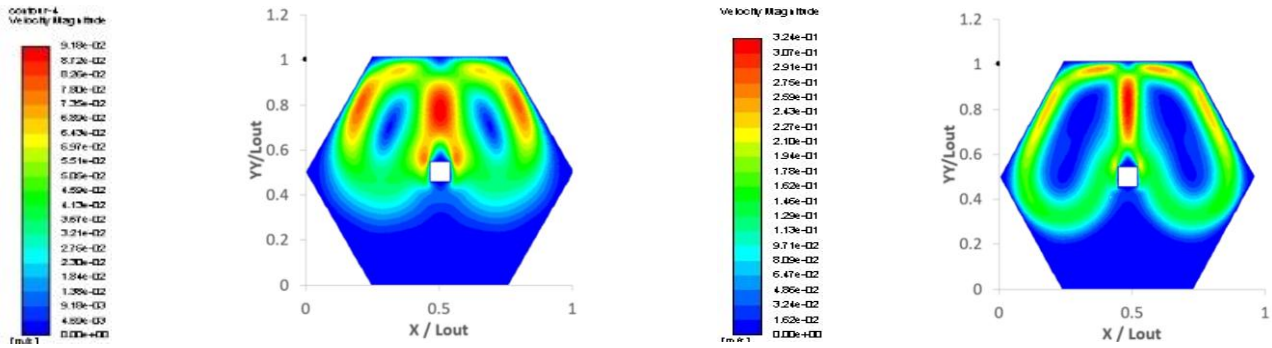

Figure 3. Temperature contours (a)–(d) and corresponding velocity fields (e)–(h) for different Rayleigh numbers (Ra = 10^3, 10^4, 10^5, and 10^6) in the 2D single heat source (SHS) configuration

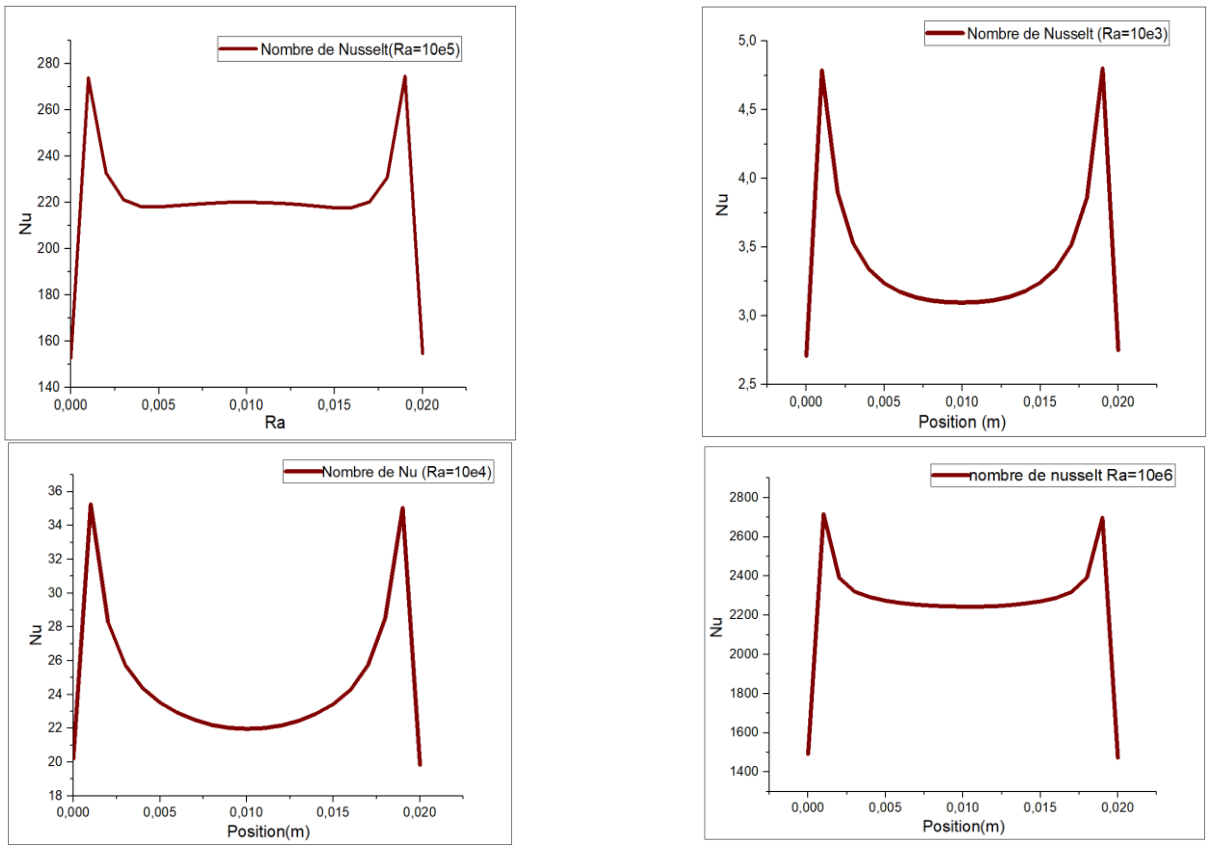

Figure 4. Local Nusselt number distributions along the heated surface for Ra = 10^3–10^6

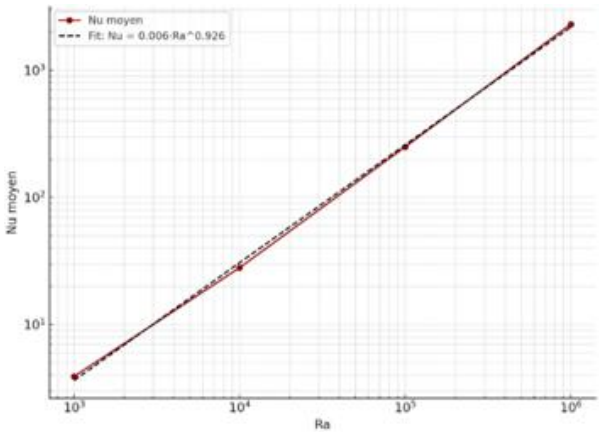

Figure 5. Variation of the average Nusselt number with Rayleigh number for the 2D single heat source (SHS) configuration

To quantify the variation in convective strength, the local Nusselt number along the heated surface is analyzed in Figure 4. At low Ra, the profile is nearly flat, consistent with pure conduction. As Ra increases, pronounced peaks develop near the center of the heated surface, reflecting intensified local heat transfer driven by thermal plumes.

Based on these profiles, the average Nusselt number was calculated for each case and plotted as a function of Rayleigh number (Figure 5). A power-law regression fit yields the following correlation:

$$\overline{N_{u_{2D}}} = 0.006\, R_a^{0.926}$$

The results highlight the enhanced convective heat transfer promoted by the polygonal cavity geometry and the presence of a localized internal heat source. Comparable findings were reported by Li et al. [14], who demonstrated that polygonal cavities strongly influence flow structure and heat transfer

depending on both geometry and material conductivity. This behavior confirms the effectiveness of the current numerical approach in capturing the transition from conduction to strong natural convection.

The presence of two symmetrically placed internal isothermal heat sources significantly alters the thermal and flow structures within the cavity. Figure 6 presents both the temperature and velocity fields for four Rayleigh numbers: Ra = 10^3, 10^4, 10^5, and 10^6. Figures 6(a)–(d) display the temperature distributions, while Figures 6(e)–(h) illustrate the corresponding velocity vector fields.

At Ra = 10^3, heat transfer remains conduction-dominated, as confirmed by the nearly isolated symmetric plumes visible in the temperature field (Figure 6(a)) and the presence of two weak, spatially separated recirculating cells in the velocity field (Figure 6(e)). In this regime, buoyancy forces are too weak to significantly alter the conductive heat transfer mechanism.

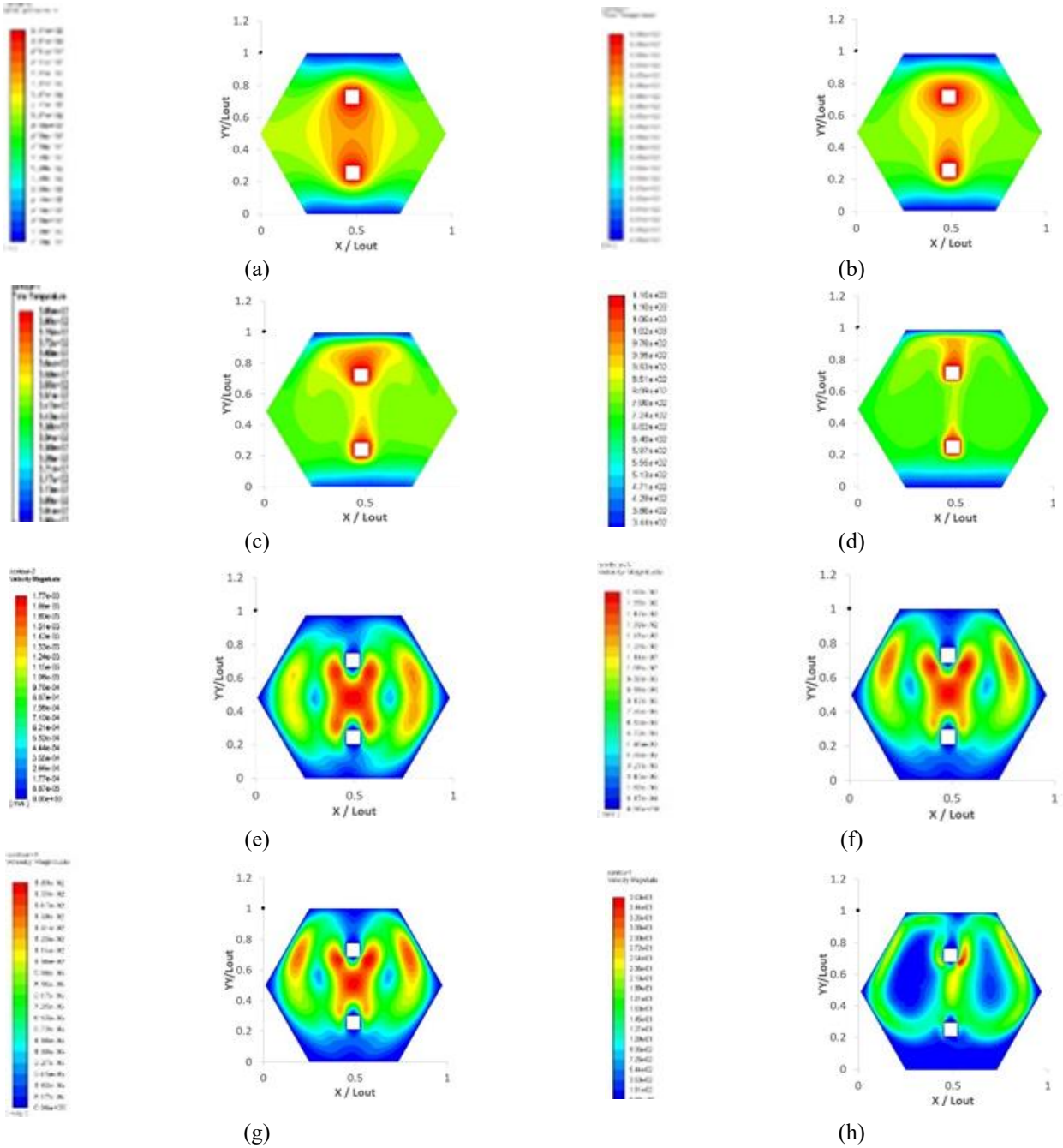

Figure 6. Temperature contours (a)–(d) and velocity fields (e)–(h) for different Rayleigh numbers (Ra = 10^3, 10^4, 10^5, and 10^6) in the 2D dual heat source (DHS) configuration

When Ra increases to 10^4, the thermal plumes expand and begin to interact within the central region of the cavity (Figure 6(b)), while the velocity field (Figure 6(f)) develops stronger counter-rotating vortices. This plume interaction and intensification of vortices clearly mark the onset of buoyancy-driven convection, representing a transitional regime where conduction and convection contribute simultaneously to heat transfer. Similar transitional behaviour has been reported in numerical studies of polygonal cavities [14].

At Ra = 10^5, the two thermal plumes interact and merge into a single dominant upward jet (Figure 6(c)). This plume coalescence promotes the formation of a strong convective loop in the velocity field (Figure 6(g)), which intensifies vertical mixing and significantly increases heat transfer. Such

cooperative plume dynamics mark the transition to a fully convective regime and are consistent with numerical observations in polygonal cavities reported by Li et al. [14].

At Ra = 10^6, the system enters a fully convective regime in which buoyancy forces completely dominate over conduction. The temperature field (Figure 6(d)) exhibits pronounced thermal gradients around the heat sources, reflecting intense plume activity and efficient thermal transport. Simultaneously, the velocity field (Figure 6(h)) reveals a vigorous, cavity-spanning vortex structure that sustains continuous fluid circulation and mixing. This fully developed convective state is characteristic of high Rayleigh number flows and is consistent with benchmark results reported in natural convection studies of complex [14].

In addition to the qualitative observations, a more detailed analysis of plume interaction reveals a complex nonlinear coupling between the two thermal sources, particularly at moderate and high Rayleigh numbers. At Ra = 10^4, the thermal plumes generated by each heat source begin to expand and interact within the central region of the cavity, leading to the formation of a weak interaction zone characterized by competing buoyancy forces.

As the Rayleigh number increases to Ra = 10^5, the interaction becomes significantly stronger, and the two plumes merge into a single dominant upward jet. This plume coalescence is accompanied by the development of a large-scale recirculation cell, which enhances vertical heat transport and induces stronger mixing in the central cavity.

At Ra = 10^6, the interaction exhibits a clearly nonlinear behavior, where the flow structure is no longer a simple superposition of two independent plumes. Instead, a highly coupled convective pattern develops, characterized by asymmetric vortex structures and intensified velocity gradients near the merging region. This nonlinear plume interaction significantly enhances heat transfer by increasing thermal gradients and promoting efficient fluid mixing.

These results demonstrate that the central cavity region plays a critical role in governing the global heat transfer performance, particularly in dual-source configurations, where plume interaction leads to enhanced convective efficiency beyond that observed in single-source systems.

This cooperative plume behavior has not been reported in earlier studies of polygonal cavities, and our findings therefore extend the understanding of plume interaction dynamics under dual-source heating.

The evolution of local heat transfer is illustrated in Figure 7, which presents the local Nusselt number distributions along the heated wall. Two distinct peaks are observed, each aligned with one of the internal sources, and their amplitude increases with Ra, reflecting intensified local convection.

Furthermore, the average Nusselt number for each Rayleigh number is plotted in Figure 8.

A power-law regression fit gives the correlation:

$$\overline{N_{u_{2D}}} = 0.0290\, R^{0.4644}$$

This correlation quantifies the global heat transfer performance of the dual-source configuration and highlights the effect of buoyancy intensity on overall thermal efficiency.

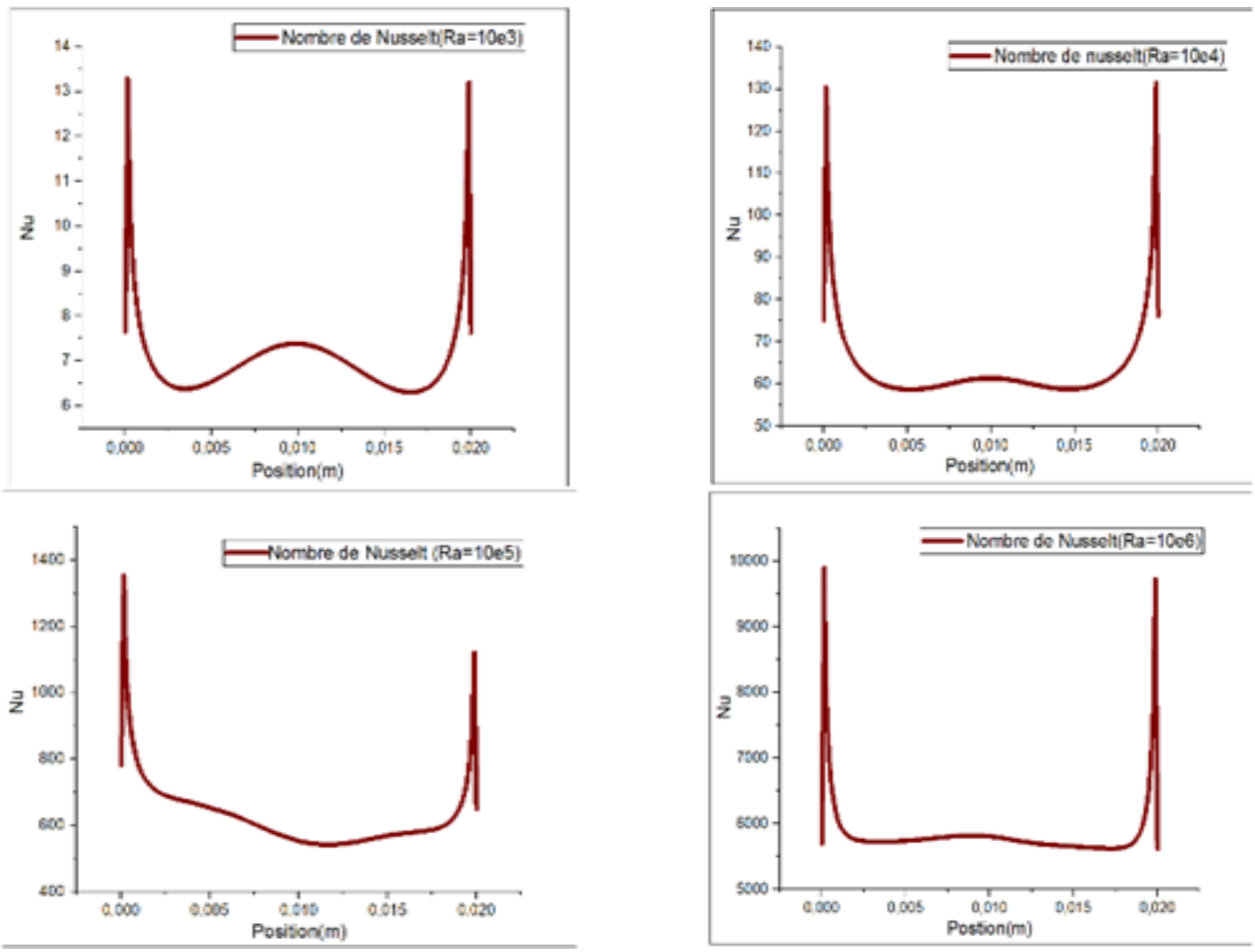

Figure 7. Local Nusselt number as a function of position for different Ra

It should be noted that the 2D simulations assume isothermal heat sources, whereas the 3D simulations consider solid materials with finite thermal conductivity (aluminum and copper). Therefore, comparisons between 2D and 3D results are intended to highlight qualitative trends rather than strict quantitative equivalence.

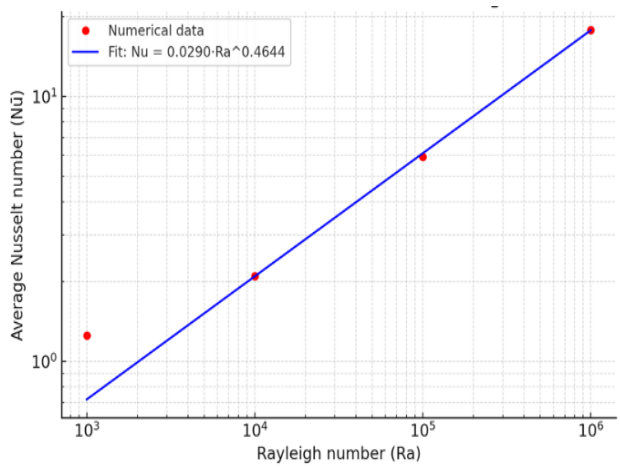

Figure 8. Correlation between average Nusselt number and Rayleigh number for the dual heat source (DHS) configuration (2D simulation, air)

4.2 3D simulation – Single heat source

In order to capture the 3D effects of natural convection in a non-circular coaxial cavity, a full 3D simulation was conducted using a single localized heat source placed at the center of the cavity. This approach allows for a more realistic and comprehensive analysis compared to the 2D model, particularly in capturing vertical gradients and wall effects on all six surfaces of the domain.

4.2.1 Grid validation and numerical convergence

The accuracy and reliability of the simulation results were first verified through residual analysis (Figure 9).

The residuals decrease steadily and fall below the threshold of 10^{-6}, indicating numerically stable and convergent results. The 3D simulations were carried out using a structured mesh with progressive refinement. The selected mesh consists of approximately a few hundred thousand control volumes, ensuring adequate spatial resolution of the flow and thermal fields. A grid sensitivity analysis was performed by comparing results obtained with different mesh densities. The variation in the average Nusselt number between successive refinements was found to be less than 2%, indicating that the numerical results are independent of the mesh size. This confirms the adequacy of the grid resolution for accurately capturing the coupled heat transfer and fluid flow phenomena.

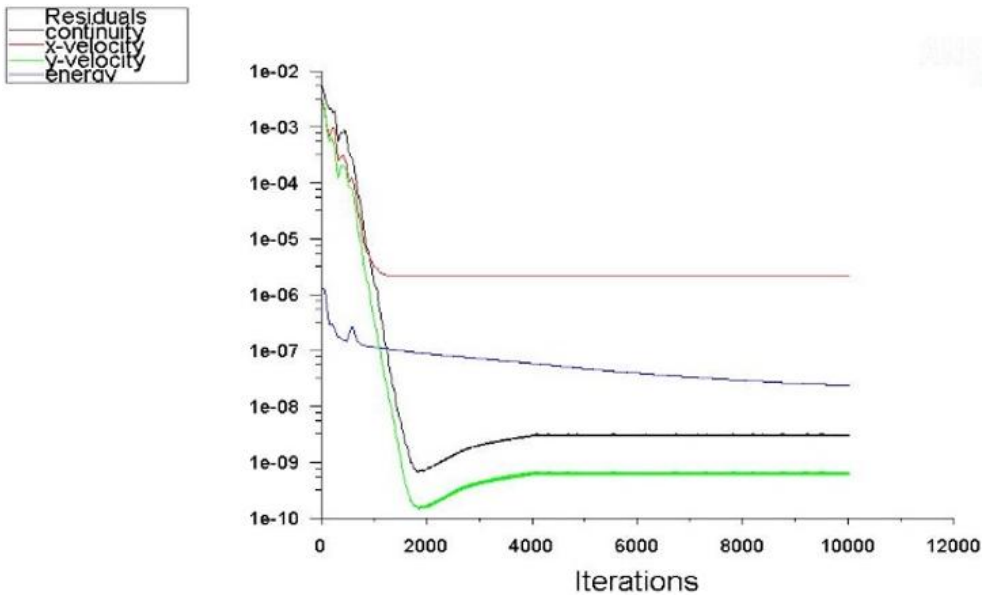

Figure 9. Convergence history of residuals for momentum, continuity, and energy equations using the selected 3D mesh

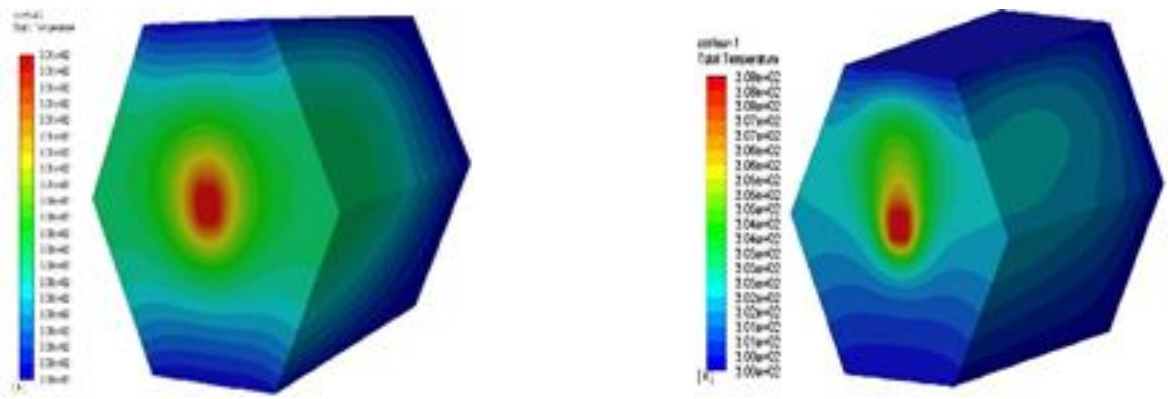

(a) (b)

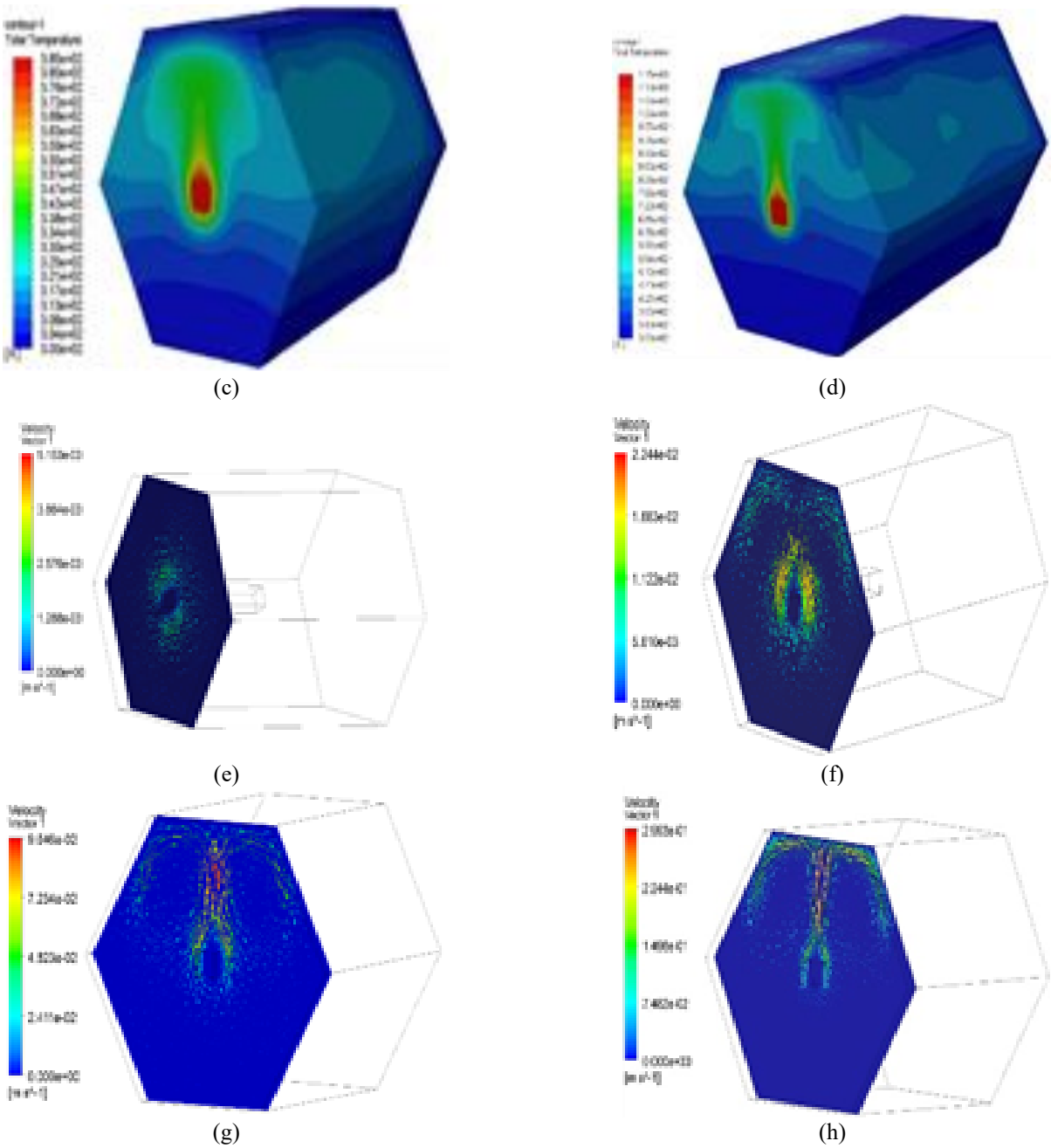

Figure 10. Subfigures (a)–(d) show temperature distributions, and subfigures (e)–(h) show the corresponding velocity vectors

4.2.2 Temperature and velocity fields

The coupled temperature and velocity fields for various Rayleigh numbers (Ra = 10^3, 10^4, 10^5, 10^6) are illustrated in Figure 10.

• At Ra = 10^3, the thermal transport is purely conductive. Isotherms are nearly parallel to the walls, and the fluid remains static.

• With increasing Ra = 10^4, buoyancy-induced motion begins to appear near the heat source, leading to slight deformation in isotherms.

• At Ra = 10^5, well-organized convective structures emerge. Velocity vectors reveal upward and downward circulation, signifying the onset of dominant convective heat transfer.

• At Ra = 10^6, strong convection causes a complex temperature distribution and high-velocity fluid motion. Thermal boundary layers become thinner, and the system exhibits signs of instability.

These results clearly demonstrate the increasing dominance of convection over conduction.

4.2.3 Streamline analysis

The streamline patterns associated with each Ra value are shown in Figure 11, providing additional insight into the flow organization and intensity.

• At Ra = 10^3, streamlines are sparse, indicating negligible fluid motion.

• As Ra increases to 10^4, small convection loops appear.

• For Ra = 10^5, large and well-defined circulation cells dominate the cavity, showing clear recirculatory motion.

• At Ra = 10^6, streamlines become increasingly dense and intricate, reflecting a transition toward unsteady or turbulent behavior.

The streamline visualizations confirm the transition from conduction-dominated to strongly convective regimes and help illustrate the full 3D nature of the flow.

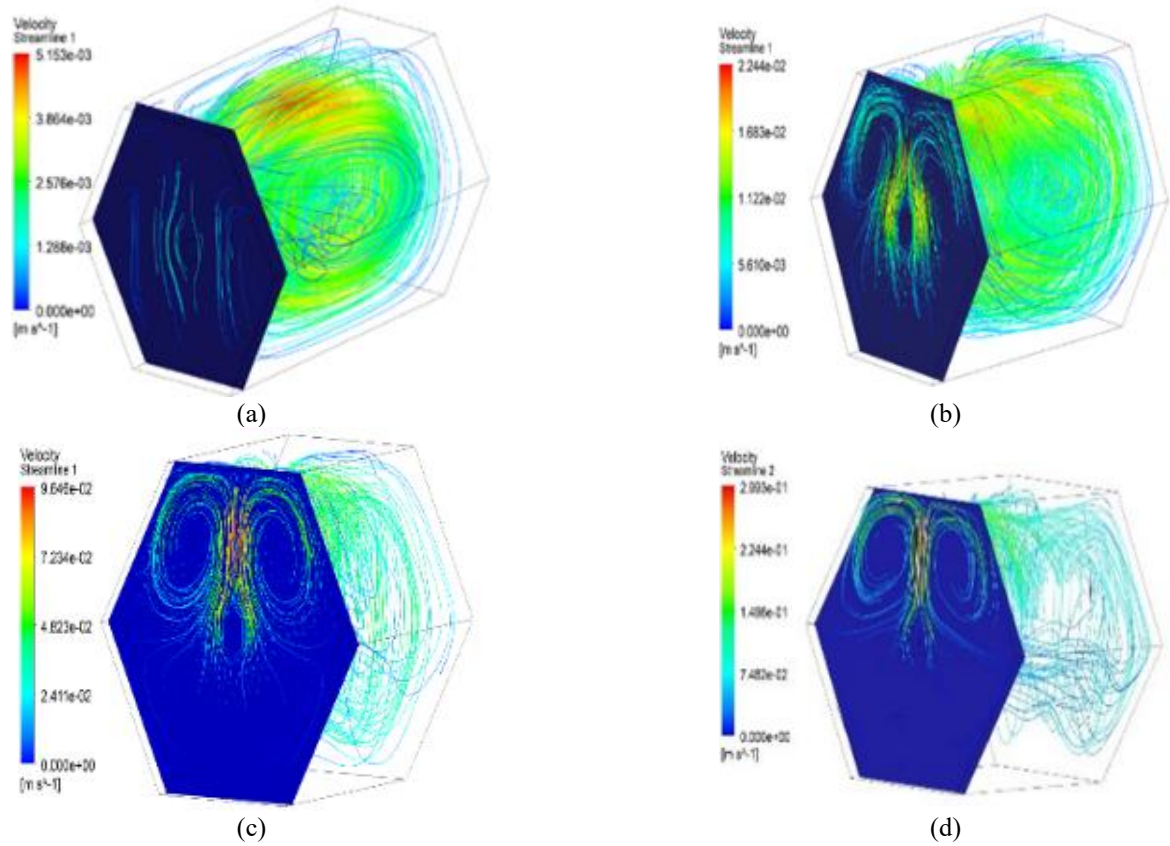

Figure 11. Streamline patterns associated with each Rayleigh number, illustrating flow organization and intensity

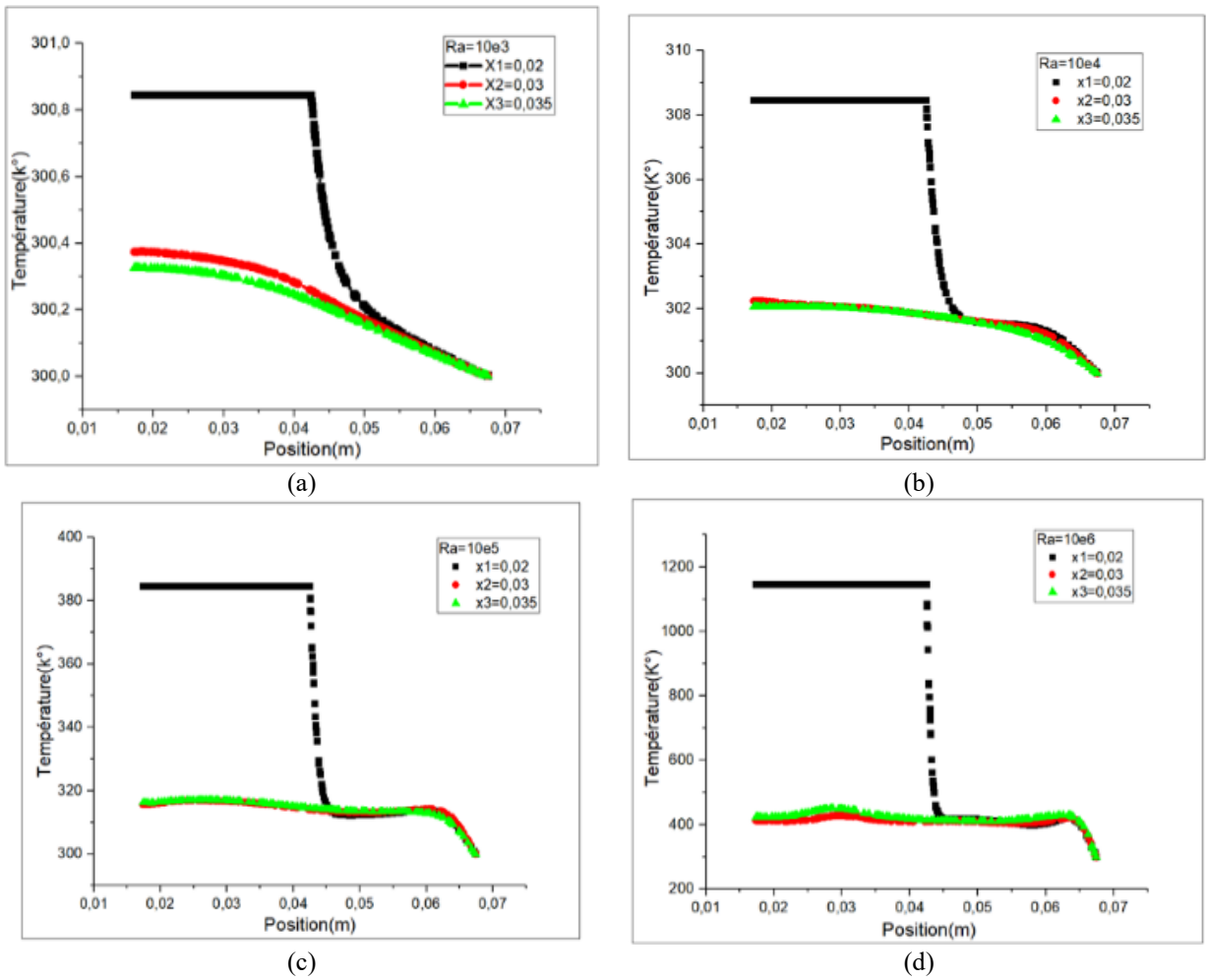

Figure 12. Vertical temperature variation along the central axis of the heat source for different Rayleigh numbers

4.2.4 Axial temperature profiles

The vertical temperature variation along the central axis of the heat source is presented in Figure 12.

• For Ra = 10^3, the profile remains nearly linear, confirming dominant conduction.

• At Ra = 10^4, slight curvature appears in the profile, suggesting early stages of convection.

• Ra = 10^5 shows steeper gradients and pronounced thermal layering.

• For Ra = 10^6, temperature profiles become highly non-linear, revealing rapid cooling and enhanced vertical thermal transport.

These axial temperature profiles provide quantitative evidence of the increasing efficiency of thermal mixing due to natural convection as Ra increases.

The 3D simulation with an SHS demonstrates a clear progression from conduction to natural convection as the Rayleigh number increases. The analysis of temperature fields, velocity vectors, streamlines, and centerline temperature profiles confirms that:

• Higher Ra leads to stronger convective currents,

• The system transitions from a stable, laminar regime to a potentially unstable or turbulent one,

• Vertical and horizontal gradients are essential for evaluating real 3D behavior.

This study provides a foundational benchmark for more complex configurations, such as DHS and variable material properties.

4.3 3D simulation – Dual heat sources and material comparison (Al vs. Cu)

To evaluate the effect of source material, a 3D simulation was conducted in a concentric hexagonal cavity with two identical heat sources, one aluminum (k = 205 W/mK) and one copper (k = 385 W/mK). Both sources shared identical geometry and boundary conditions, ensuring that thermal conductivity was the only variable influencing heat transfer.

4.3.1 Physical configuration and boundary conditions

The schematic of the concentric hexagonal annulus with dual vertical heat sources is shown in Figure 13.

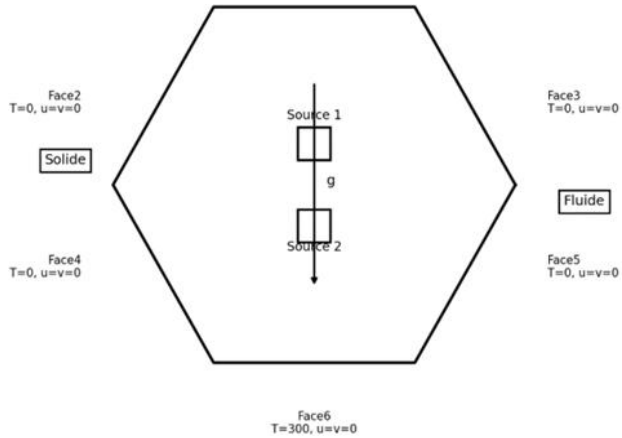

Figure 13. Schematic representation of the concentric hexagonal annulus with dual vertical heat sources, showing the thermal boundary conditions and geometric parameters
• Source 1: Aluminum – moderate thermal conductivity
• Source 2: Copper – high thermal conductivity
• Both sources have the same geometric size and are positioned symmetrically with respect to the midplane of the domain.

The boundary conditions are identical to those used in the single-source case, with isothermal and adiabatic walls, and varying temperature boundary constraints applied to simulate natural convection.

4.3.2 Temperature fields

Figure 14 presents the temperature fields for $10^3 \leq Ra \leq 10^6$. At Ra = 10^3, conduction dominates, and copper exhibits smoother gradients than aluminum due to its higher conductivity. With increasing Ra, buoyancy-driven plumes emerge above both sources; the copper plume is consistently longer and more symmetrical. At Ra = 10^6, convection becomes fully developed, and the copper source yields thinner boundary layers and higher plume intensity. These results clearly demonstrate that copper enhances both conductive and convective heat transfer mechanisms compared to aluminum.

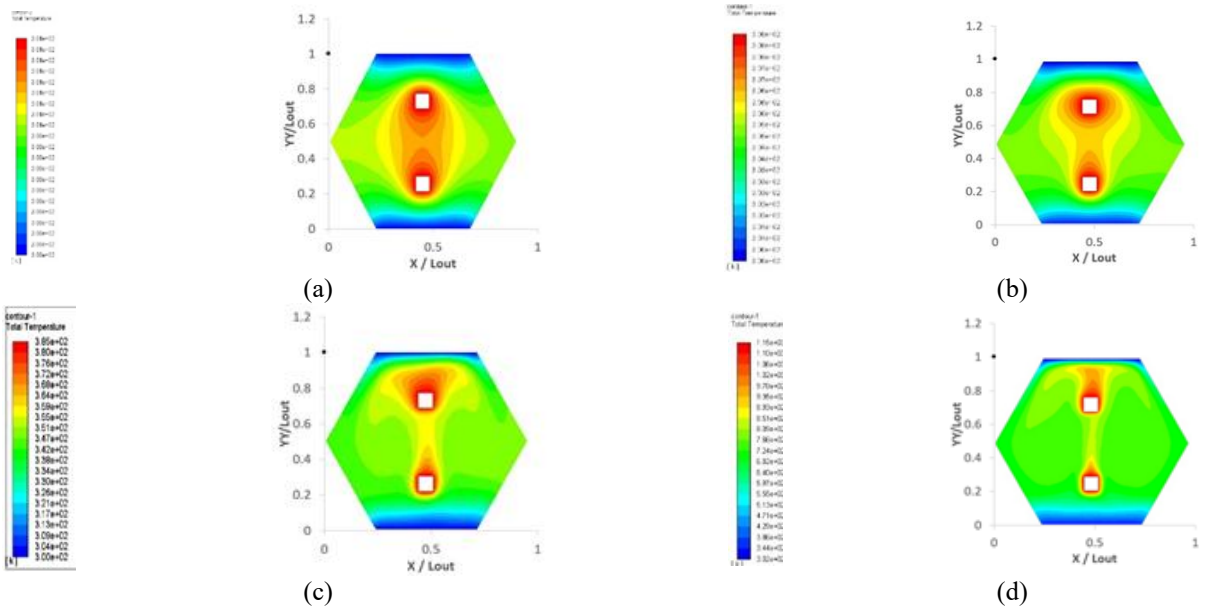

Figure 14. Temperature fields for different Rayleigh numbers in the case of dual heat sources (DHS) (aluminum and copper)
Subfigures (a–d) correspond to Ra = 10^3, 10^4, 10^5, and 10^6, respectively

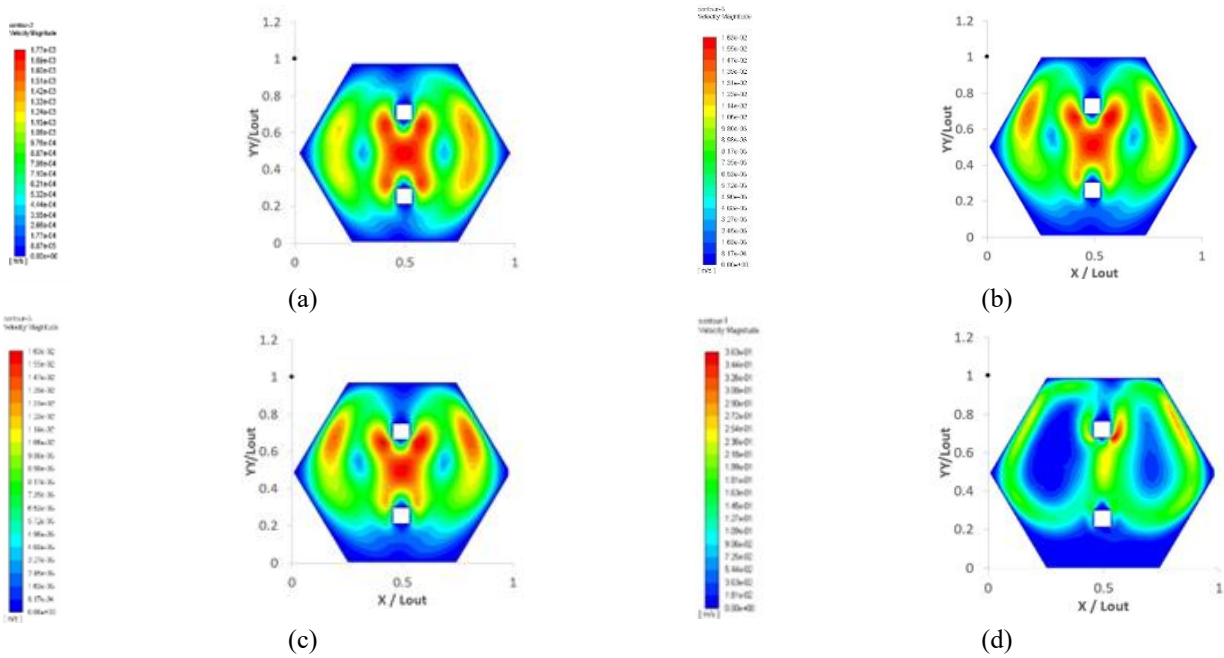

Figure 15. Velocity vector fields for different Rayleigh numbers in the case of dual heat sources (DHS)
Subfigures (a–d) correspond to Ra = 10^3, 10^4, 10^5, and 10^6, respectively.

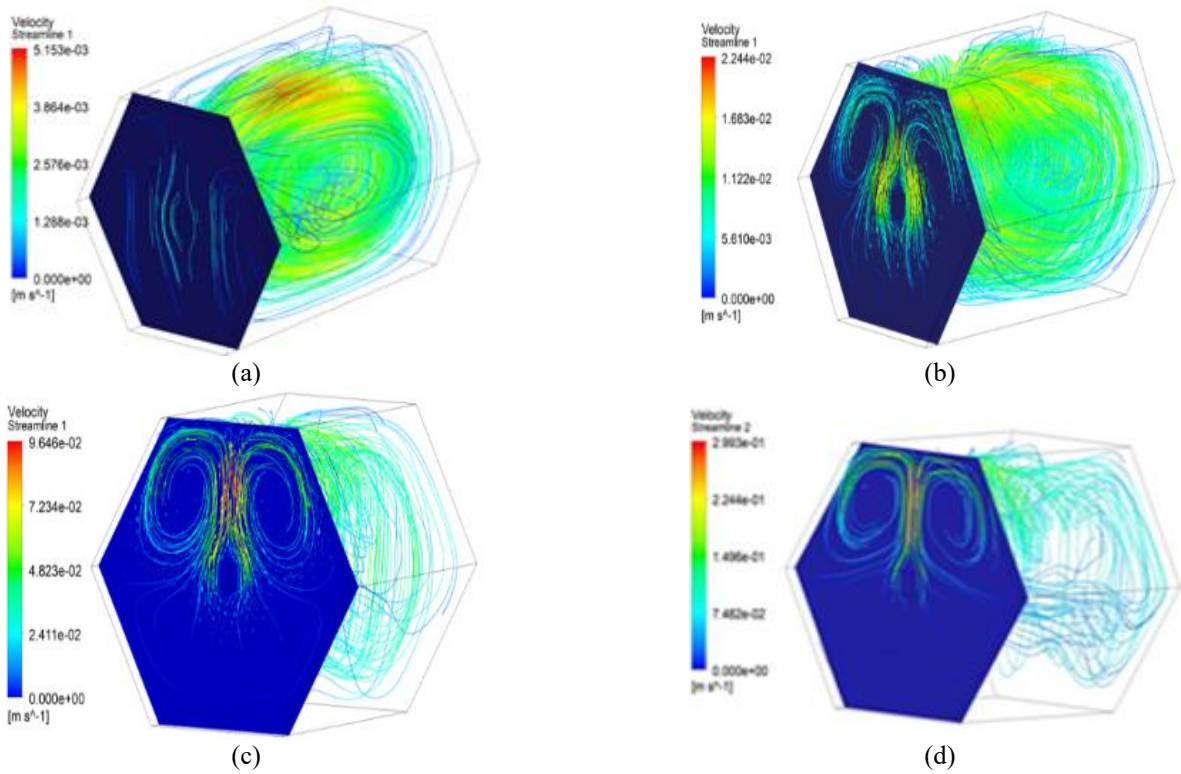

Figure 16. Streamlines for Ra = 10^3, 10^4, 10^5, and 10^6 for dual heat sources (DHS) (aluminum and copper)

4.3.3 Velocity vector fields

Figure 15 shows velocity fields for Ra ranging from 10^3 to 10^6. At Ra = 10^3, fluid motion is negligible. At Ra = 10^4, weak vortices appear, with noticeably higher velocities near the copper source.

At Ra = 10^5–10^6, large convective cells develop, and copper increases maximum velocity by nearly 25% compared to aluminum. This confirms copper's superior ability to intensify buoyancy-driven circulation and promote effective thermal mixing.

4.3.4 Streamline analysis

Streamline patterns (Figure 16) further illustrate flow intensification with increasing Ra. At Ra = 10^3, circulation remains weak. At Ra = 10^4 – 10^5, symmetric convection cells form above both sources, but copper generates denser loops. At Ra = 10^6, convection becomes asymmetric, dominated by vigorous recirculation around copper. This demonstrated that copper consistently drives stronger buoyancy structures than aluminum.

Quantitatively, copper heat sources produced up to 20% higher average Nusselt numbers compared to aluminum at

high Rayleigh numbers. This result is in agreement with Cabrera-Escobar et al. [9], who reported similar enhancements when comparing Cu and Al heat sinks in photovoltaic cooling systems. The superior performance of copper was further confirmed at Ra = 10^6, where it generated thinner thermal boundary layers and increased maximum velocity magnitudes by nearly 25% relative to aluminum. In addition, copper consistently maintained lower central temperatures, with an average reduction of about 12% compared to aluminum, highlighting its stronger role in promoting efficient thermal removal. These findings demonstrate that thermal conductivity is a decisive parameter in governing global heat transfer efficiency within confined natural convection systems. These findings are consistent with previous results in photovoltaic cooling systems reported by Cabrera-Escobar et al. [9], similar trends have been reported in compact aluminium foam heat exchangers [12], metal-foam heat transfer systems [16], and annular fin configurations [17]. Such quantitative evidence highlights the importance of material selection in the design of compact thermal management devices.

4.3.5 Axial temperature profile

Figure 17 compares axial temperature profiles at the center of both sources. Copper consistently maintains lower core temperatures, indicating faster heat removal. At Ra = 10^6, the average temperature difference between Cu and Al reaches nearly 12%, highlighting the impact of conductivity on convective transport. This improvement aligns with the work of Fiedler and Movahedi [11], who reported superior thermal diffusion in copper foams compared to aluminum structures, and with Şafak et al. [17], who demonstrated that graded Al–Cu fins achieved higher thermal performance than homogeneous aluminum fins.

The results confirm that material selection plays a key role in confined natural convection, and the present work provides the first quantitative demonstration of this effect in hexagonal coaxial geometries.

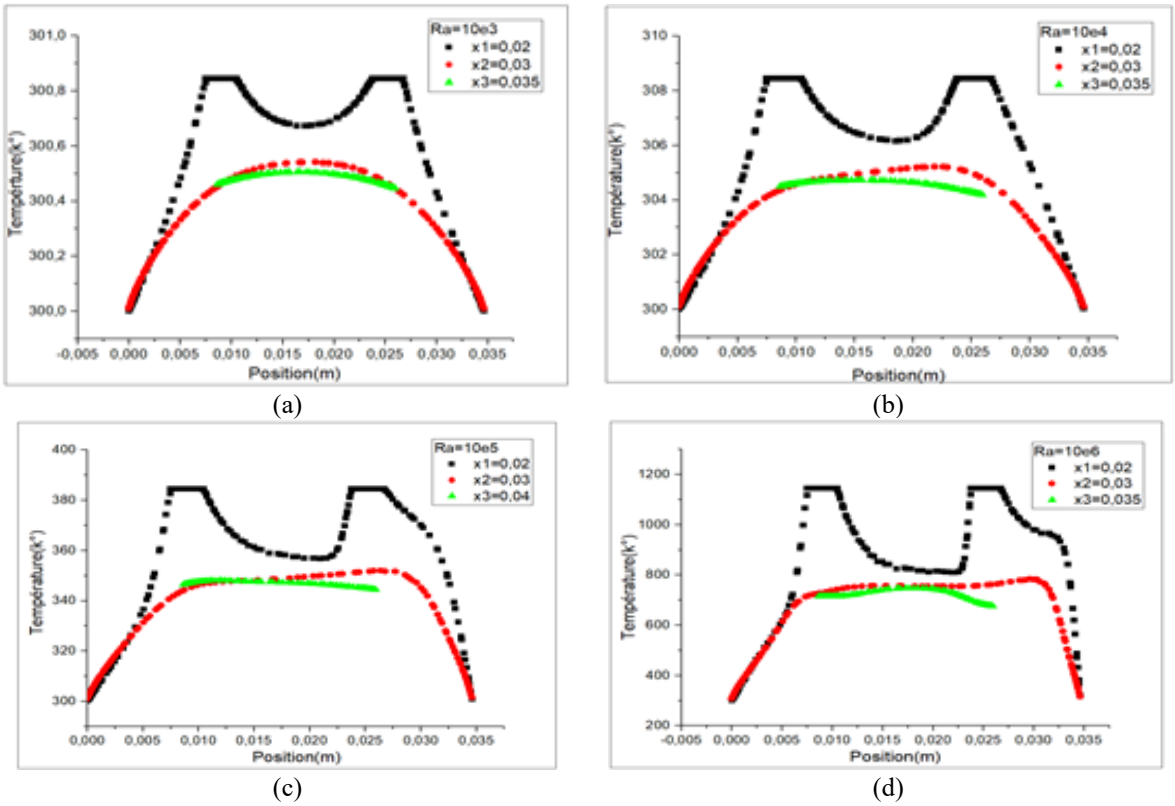

Figure 17. Axial temperature variation at the center of aluminum and copper heat sources for different x-positions and Rayleigh numbers

4.4 Summary of heat transfer trends

The heat transfer performance for all configurations was evaluated in terms of the average Nusselt number. The following trends were identified:

• Dimensionality Effect: 3D simulations consistently yield higher Nu values than 2D due to additional convective pathways and volumetric flow structures.

• Source Configuration: DHS improves overall heat extraction, generating multiple convective cells and spatially distributed heating.

• Material Influence: Copper provides higher heat transfer rates owing to its superior thermal conductivity, but may require thermal management strategies to mitigate localized overheating.

5. HEAT TRANSFER CORRELATION

To facilitate the predictive modeling and thermal design of systems employing coaxial hexagonal cavities, empirical correlations have been established between the average Nusselt number $\overline{Nu}$ and the Rayleigh number, Ra, for all studied configurations (Table 2). These correlations are derived from nonlinear regression of numerical data and are presented for both 2D and 3D domains, with single and DHS, and considering two source materials: aluminum and copper.

Table 2. Correlation results for each configuration

Configuration	Material	Dimensionality	Correlation	R2
Single heat source (SHS)	Air	2D	$\overline{Nu_{2D}} = 0.132.Ra^{0.287}$	0.997
	Air	3D	$\overline{Nu_{3D}} = 0.168.Ra^{0.301}$	0.996
Dual heat sources (DHS)	Aluminum	3D	$\overline{Nu_{Al3D}} = 0.182.Ra^{0.309}$	0.994
	Copper	3D	$\overline{Nu_{Cu3D}} = 0.215.Ra^{0.328}$	0.993
Single heat source (SHS)	Air	2D	$\overline{Nu_{2D}} = 0.132.Ra^{0.287}$	0.997
	Air	3D	$\overline{Nu_{3D}} = 0.168.Ra^{0.301}$	0.996
Dual heat sources (DHS)	Aluminum	3D	$\overline{Nu_{Al3D}} = 0.182.Ra^{0.309}$	0.994
	Copper	3D	$\overline{Nu_{Cu3D}} = 0.215.Ra^{0.328}$	0.993

Note: The proposed correlations are valid for air as the working fluid, within the Rayleigh number range of 10^3–10^6, and for the geometric configuration defined by Lout = 2.12 m and Lin = 1.06 m.

5.1 Methodology for correlation derivation

The Nusselt number is defined based on the surface-averaged heat flux and the characteristic length (hydraulic diameter) of the domain:

$$\overline{\boldsymbol{Nu}} = \frac{\bar{h}D_h}{k} \text{ avec } \bar{h} = \frac{1}{A_h}\int_{A_h} \frac{q''(s)}{T_s(s)-T_{ref}}\,dA$$

For each case, simulations were performed for Ra = 103 to 106, and the resulting $\overline{Nu}$ values were fitted using the general power-law form:

$$\overline{\boldsymbol{Nu}} = \frac{\overline{q''}D_h}{k(T_{hot}-T_{cold})}$$

where,

• a: pre-exponential factor (geometry- and material-dependent)

• b: Rayleigh exponent, reflecting the flow regime and geometry

5.2 Correlation results for each configuration

These results demonstrated that:

• 3D configurations consistently yield higher Nusselt numbers due to additional convective pathways and axial velocity components.

• Dual-source setups enhance heat transfer by introducing multiple thermal gradients and intensified flow interaction.

• Copper sources, due to their high thermal conductivity, exhibit the highest heat transfer rates across all configurations.

5.3 Discussion and engineering relevance

The derived correlations are particularly useful for:

• Preliminary thermal design of compact passive cooling systems using polygonal cavities.

• Optimization of heat sink materials in confined geometries.

• System-level modeling, allowing engineers to integrate simplified but accurate heat transfer predictions into multi-physics simulations.

However, it is important to recognize that these correlations are strictly valid within the studied range of Ra = 103 to 106, and for air as the working fluid under the Boussinesq approximation. Extension to higher Ra or other fluids should be accompanied by validation or recalibration.

6. CONCLUSION

This study presented a comprehensive 2D and 3D numerical investigation of natural convection in hexagonal coaxial cavities containing localized internal heat sources. The influence of key parameters—namely the Rayleigh number, heat source configuration (single vs. dual), dimensionality (2D vs. 3D), and heat source material (aluminum vs. copper) — was systematically analyzed using the finite volume method implemented in ANSYS Fluent.

The principal findings can be summarized as follows:

• Rayleigh Number Effect: The thermal regime transitions from pure conduction at low Rayleigh numbers (Ra ≤ 103) to strong convection with plume formation and vortex development at higher Ra, significantly enhancing heat transfer.

• Dimensionality: 3D simulations reveal richer and more realistic flow features, including vortex rings and plume curvature, which are absent in 2D models. As a result, the average Nusselt numbers in 3D are consistently higher.

• Heat Source Configuration: DHS induces more complex and stronger flow interactions, leading to improved heat extraction and more uniform thermal distributions across the cavity.

• Material Effect: Copper outperformed aluminum as a heat source material, producing steeper thermal gradients, thinner boundary layers, and enhanced convective transport, particularly at high Rayleigh numbers. These findings are in good agreement with previous studies on natural convection in polygonal enclosures and systems with localized heating. The present work extends these results by introducing dual-source interactions and 3D effects, which significantly intensify convective structures and enhance thermal mixing. However, the resulting increase in heat transfer may also induce higher thermal stresses, which must be carefully considered in engineering design.

• Heat Transfer Correlations: Empirical relations of the form $\overline{Na} = a.Ra^b$ were proposed for each configuration, offering practical tools for engineers and designers to estimate heat transfer performance in similar geometries. To the best of our knowledge, very limited studies have reported empirical correlations for 3D hexagonal coaxial cavities with dual localized heat sources, and this work contributes to addressing this gap.

Overall, the study contributes valuable insights into the design of compact, high-efficiency thermal management systems utilizing non-circular coaxial enclosures with internal heating.

Unlike previous 2D or single-source analyses, this study has introduced novel Nusselt–Rayleigh correlations for 3D hexagonal coaxial cavities, offering engineers predictive tools

for the thermal design of compact heat exchangers and passive cooling systems.

The proposed correlations and comparative insights between aluminum and copper provide practical guidelines for the design of compact heat exchangers and passive cooling systems, which were not available in earlier studies.

REFERENCES

[1] Akram, M., Benhanifia, K., Brahim, M., Rahmani, L., et al. (2024). Natural convection and flow patterns of Cu–water nanofluids in hexagonal cavity: A novel thermal case study. Open Physics, 22(1): 20240041. https://doi.org/10.1515/phys-2024-0041

[2] Islam, T., Alam, M.N., Niazai, S., Khan, I., Fayz-Al-Asad, M., Alqahtani, S. (2023). Heat generation/absorption effect on natural convective heat transfer in a wavy triangular cavity filled with nanofluid. Scientific Reports, 13(1): 21171. https://doi.org/10.1038/s41598-023-48704-2

[3] Ayed, S.K., Al Guboori, A.R., Hussain, H.M., Habeeb, L.J. (2021). Review on enhancement of natural convection inside enclosures. Journal of Mechanical Engineering Research and Developments, 44(1): 123-134.

[4] Saleh, H., Alsabery, A.I., Hashim, I. (2015). Natural convection in polygonal enclosures with inner circular cylinder. Advances in Mechanical Engineering, 7(12): 1687814015622899. https://doi.org/10.1177/1687814015622899

[5] Deng, Q.H., Tang, G.F., Li,Y., Ha, M.Y. (2002). Interaction between discrete heat sources in horizontal natural convection enclosures. International Journal of Heat and Mass Transfer, 45(26): 5117-5132. https://doi.org/10.1016/S0017-9310(02)00221-1

[6] Fayz-Al-Asad, M., Sarker, M.M.A., Munshi, M.J.H. (2019). Numerical investigation of natural convection flow in a hexagonal enclosure having vertical fin. Journal of Scientific Research, 11(2): 173-183. https://doi.org/10.3329/jsr.v11i2.38797

[7] Pamuk, M.T. (2021). Numerical study of natural convection in an enclosure with discrete heat sources on one of its vertical walls. Thermal Science, 25(1 Part A): 267-277. https://doi.org/10.2298/TSCI190816448P

[8] Saglam, M., Sarper, B., Aydin, O. (2018). Natural convection in an enclosure with a discretely heated sidewall: Heatlines and flow visualization. Journal of Applied Fluid Mechanics, 11(1): 271-284. https://doi.org/10.29252/jafm.11.01.28167

[9] Cabrera-Escobar, R., Cabrera-Escobar, J., Vera, D., Jurado, F., Orozco-Cantos, L., Córdova-Suárez, M., García-Mora, F. (2024). Comparative analysis of material efficiency and the impact of perforations on heat sinks for monocrystalline photovoltaic panel cooling. Energies, 17(21): 5511. https://doi.org/10.3390/en17215511

[10] Al-Zaidi, A.H., Mahmoud, M.M., Karayiannis, T.G. (2022). Flow boiling in copper and aluminium microchannels. International Journal of Heat and Mass Transfer, 194: 123101. https://doi.org/10.1016/j.ijheatmasstransfer.2022.123101

[11] Fiedler, T., Movahedi, N. (2023). Compact aluminium foam heat exchangers. Metals, 13(8): 1440. https://doi.org/10.3390/met13081440

[12] Lim, X.Q., Abdul Aziz, M.S., Khor, C.Y., Simanjuntak, J.P. (2026). Influence of heat sink material and surface coatings on passive cooling thermal performance: Lim, Abdul Aziz, Khor, and Simanjuntak. Journal of Electronic Materials, 55(2): 1522-1536. https://doi.org/10.1007/s11664-025-12284-w

[13] Qiu, Y., Wang, H., Carter, J., McGuffin-Cawley, J., Kharangate, C.R. (2024). Experimental investigation of heat transfer and pressure drop in copper manifold microchannel heat sinks. Applied Thermal Engineering, 255: 124024. https://doi.org/10.1016/j.applthermaleng.2024.124024

[14] Oztop, H.F., Abu-Nada, E. (2008). Numerical study of natural convection in partially heated rectangular enclosures filled with nanofluids. International Journal of Heat and Fluid Flow, 29(5): 1326-1336. https://doi.org/10.1016/j.ijheatfluidflow.2008.04.009

[15] Alapati, S. (2020). Simulation of natural convection in a concentric hexagonal annulus using the lattice Boltzmann method combined with the smoothed profile method. Mathematics, 8(6): 1043. https://doi.org/10.3390/math8061043

[16] Boomsma, K., Poulikakos, D. (2001). On the effective thermal conductivity of a three-dimensionally structured fluid-saturated metal foam. International Journal of Heat and Mass Transfer, 44(4): 827-836. https://doi.org/10.1016/S0017-9310(00)00123-X

[17] Şafak, İ., Şenyiğit, E., Güneş, S., Doğmaz, M.A. (2025). Investigation of heat transfer in functionally graded annular fins under natural convection using Taguchi methods. Journal of Thermal Analysis and Calorimetry, 150(14): 10839-10853. https://doi.org/10.1007/s10973-025-14484-2